Silver/reduced graphene oxide nanocomposite materials synthesized via a green molecular level mixing

Jean-François Silvain, Benjamin Thomas, Loïc Constantin, Maël Pontoreau, Yongfeng Lu, Jean-Luc Grosseau-Poussard, Guillaume Lacombe

Silver/Reduced Graphene Oxide Nanocomposite Materials Synthesized Via a Green Molecular Level Mixing

Jean-François Silvain[1,2]*, Benjamin Thomas[1], Loic Constantin[1,2], Maël Pontoreau[1], Yongfeng Lu[2], Jean-Luc Grosseau-Poussard[3] and Guillaume Lacombe[4]

[1] Univ. Bordeaux, CNRS, Bordeaux INP, ICMCB, UMR 5026, 33600 Pessac, France
[2] Department of Electrical and Computer Engineering, University of Nebraska-Lincoln, Lincoln, NE 68588-0511, USA
[3] LaSIE UMR-CNRS 7356, Pole Science et Technologie, Université de La Rochelle, Av. M. Crépeau, 17042 La Rochelle Cedex, France
[4] Composite Innovation SAS., Parc scientifique Unitec 1, 2 all du doyen Georges brus, 33600 Pessac, France.

* Correspondance : jean-francois.silvain@icmcb.cnrs.fr

Abstract: The fabrication of nano reinforced metal matrix composites (MMCs) is scientifically essential to further upgrade the thermal, electrical, and mechanical properties of current MMCs. Here, we present a green molecular mixing (MLM) of silver (Ag) and graphene (G) to overcome these challenges. Experimental results show that the green MLM allows to homogeneously mix 3 vol.% of G as observed with traditional MLM while adding a control on the oxidation steps. Metal and GO reductions can be precisely control by varying the solution temperature. Highly thermal conductivity and strong elastic modulus nanocomposites are fabricated making it an eco-friendlier mixing process.

Keywords: Composite; Ag; Graphene; Powder metallurgy; Microstructure

Introduction

The high thermal conductivity (TC) of silver (Ag, 429 W/m.K) makes it a predominant material for electronic applications. However, Ag suffers from low mechanical properties thus, withdrawing its prospective applications. A common way to promote its mechanical properties is to fabricate metal matrix composites (MMCs). The fabrication of Ag composites is often made via a metallurgic powder route owing to its simplicity, cost-effectiveness, net shaping, and ability to manufacture anisotropic materials [1]. Oxides and graphite reinforcement have been extensively studied to enhancement the mechanical and thermal properties of Ag matrix. However, it was reported that the addition of oxides lowers the thermal conductivity (TC) [1–5] while the presence of graphite degrades the mechanical properties [1, 6–8].

Therefore, the creation of multifunctional composed of nano-carbon reinforcement such as graphene (G) or reduced graphite oxide (rGO) may fulfill these unmet needs [9–15]. Nonetheless, the size difference between the matrix powder (i.e., micrometer, Ag) and the carbon reinforcement (i.e., nanometer, G, rGO) cause several issues during the mixing step and heterogeneous mixture are often observed. Naturally, aggregation of the nano-reinforcement led to severe degradation of the resulting nanocomposites' mechanical and thermal properties [12, 13, 16]. Hence, the mixing appears to be a crucial step to manufacture functional Ag-based nanocomposites.

Mechanical mixing e.g., balling or wet mixing have been extensively used to form homogeneous mixture of micro and nano composites [17–22]. However, mechanical mixing is a harsh process where heating, deformation, crystallization, and perception co-occurs leading to the degradation of the graphene [16, 19, 20, 22–24]. Molecular level mixing (MLM) was recently introduced as a alternative mixing method to homogeneously mix G-rGO and metal matrix powders [12, 13, 25–27]. The MLM approach consists of forming a colloidal suspension of graphene oxide (GO) in an aqueous solution with metal salt precursors. After precipitation and reduction, a homogeneous dispersion of rGO in metal powder is obtained [12, 13, 26–28]. Although the promising results observed with the MLM, this method require the use of hydrazine as the reducing agent making the MLM hard to scale up due to the environment and health concerns [12, 13, 26–28].

In this work, we developed a green MLM process to fabricate Ag/rGO using ascorbic acid (AA) instead of hydrazine. AA is known as a green harmless chemical component for the environment and health [29–31]. In addition, the used AA enables to tailor the MLM process as compared to conventional MLM. Especially, the metal and GO reductions can be separated and precisely control by only varying the solution temperature. It is demonstrated that for an rGO concentration below 3 vol.% monodisperse Ag particles are synthesized with a uniform dispersion of nano-reinforcements. Additionally, the reduction rate of GO using AA and hydrazine had been monitored by Raman spectroscopy and X-ray diffraction (XRD). It is shown that both reducing agents conduct to the same

reduction rate, making AA an excellent substitute to the hydrazine. Then, nanocomposites were fabricated by hot pressing using the synthesize powders via the green MLM. It is shown that 1 vol.% of rGO in the Ag matrix lead to a 16% increase of the elastic modulus with no degradation of the Ag's TC (395 W/m.K). The research results demonstrated that substitution of hydrazine by AA allows developing a green MLM process and add a control on the metal and GO reduction. Therefore, the developed greed MLM process enables can be easily scale up.

Methods

Synthesize of nano-composite powders

Ag and reduced rGO were synthesized via a green MLM process. For that, a Ag nitrate solution (Alfa Aesar, ACS, 99.9+ %) and graphite oxide (Knano Co., Ltd., China) were reduced using L+ ascorbic acid (AA, Acros Organics, 99%). The average lateral size and thickness of the graphite oxide are 5 μm and 5 nm, respectively. The green MLM process is the following ~~(a)~~. First, a desired amount of graphite oxide was added to 100 ml of deionized water to a concentration comprise between 5.4 10-2 g/l and 5.6 10-1 g/l to obtain a concentration of rGO in the composite powder from 0.25 to 5 vol.%. Then, the solution was then mixed with a magnetic stirrer for 5 min and placed in a tip sonicator for 1 h (Bandelin SONOPULS®) with a pulse width, frequency, and power of 0.1 s, 1 Hz and 100 W respectively, to prevent reinforcement deterioration and heating. Once the solution turn into a brown color, the suspension was diluted with AA to reach a GO concentration between 6.8 10-3 g/l to 1.4 10-1 g/l. After a maturation step of 1 h, an aqueous solution of Ag nitrate (c = 2.35 10-1 mol/l) was quickly added to the GO suspension. Once the Ag reduction by AA was completed (~ 5 min), the Ag / GO suspension was heated to 90 °C for 1 h; reduction of GO occurred by the excess of AA in solution (c =7.8 10-2 mol/l). Then, the Ag+rGO mixture was filtrated and washed three times with 100 ml deionized water and three times with 50 ml ethanol. Finally, the composite mixture was air-dried in an oven at 60 °C for 24 h. In order to evaluate the reducing power of ascorbic acid towards GO, reference powder was synthesized using hydrazine hydrate as reducing agent. The synthesis conditions of this powder are identical to the previous ones but the hydrazine hydrate was substituted to ascorbic acid (in the same concentrations).

Fabrication of Ag/rGO nanocomposites

The densification of the nanocomposite powders was carried out by hot pressing under primary vacuum (~ 1.5 10-1 mbar). The nanocomposite powders were placed in a 10 mm diameter graphite mold and sintered under a uniaxial pressure of 60 MPa and temperature and time of 650 °C and 25 min respectively. The pressure was applied when the sintering temperature was reached. After sintering, the composite materials were machined and polished for characterizations.

Characterization

The reduced GO by AA and hydrazine was characterized by XRD (PANalytical X'pert PRO MPD ®, Cu-Kα) and Raman spectroscopy (Horiba spectrometer, λ = 532 nm, 10 mW). Powder XRD diffractograms were acquired from 2θ = [3° - 38°] with a scanning speed of 0.15°/min. The density of the composite materials was measured using the Archimedes method (Sartorius Analitic® balance (d = 0.1 mg)). A scanning electron microscope (SEM, Tescan VEGA ®) was used to characterize the morphology of the composite powders and fractures of the bulk composite materials. Microstructural characterization was carried out by electron backscatter diffraction (EBSD, EDAX®, probe size 330 nm, and step of 0.1 μm). The microstructure of the nanocomposites was revealed by electro-etching in 100 g/l citric aqueous acid solution for 10 to 20 s with a DC voltage and an intensity of 6 V and 0.5 A, respectively. The deep etching was performed using the same electro-etched parameters but using 0.65 wt.% nitric acid solution as the electrolyte for 1 min.

The thermal diffusivity (TD) of the materials was measured by the laser flash method (NETZSCH LFA 457®, MicroFlash) on composites cylinders of 10 mm and 6 mm in diameter with a thickness of 5 mm at 70 °C. A graphite film was spray (KONTAKT CHEMIE graphite 33® aerosol) on the samples before measurement to reduce the laser back reflection. The TD was converted into TC using the following equation [32]:

$$k(T)=a(T)\times Cp\,(T)\times \varrho(T) \quad (1)$$

where k is the TC (W/m.K), a is the TD (mm^2/s), ϱ the density, and Cp the heat capacity (J/Kg.K) of the sample. The Cp of rGO, and Ag, used in this work, are the following: Cp(rGO) = 836 J.Kg-1.K-1 Cp(Ag) = 237 J.Kg-1.K-1 at 70 °C.

Hardness and apparent elastic modulus of materials were measured by micro-hardness measurement in the transverse direction. An indentation force of 1 N, a charging and discharging speed of 500 mN/min, and a pause time of 20 s was used for all samples. Oliver and Pharr's theory [33], [34], was used to derive the elastic modulus from the load/discharge curves of the tested composite materials.

Results & Discussion

This section may be divided by subheadings. It should provide a concise and precise description of the experimental results, their interpretation as well as the experimental conclusions that can be drawn.

Green molecule mixing of silver and reduced graphene oxide

The size difference between the Ag particles and the GO nano reinforcement makes the mixing of these two components an essential step to produce nanocomposites. A green MLM process was developed by using AA to obtain a homogeneous powder mixture at GO concentration ranging from 0.1 to 5 vol.%. The substitution of hydrazine by AA enables us to work with a green component but also to separate the precipitation/reduction of Ag particles and GO Figure 1 presents the SEM micrographs of the Ag/rGO composite powders for different rGO concentrations. It can be observed that the nucleation and growth of Ag in the aqueous suspension conducts to monodisperse particles (~2 μm) for an rGO concentration up to 3 vol.% (Figure 1 (a) to (c)).

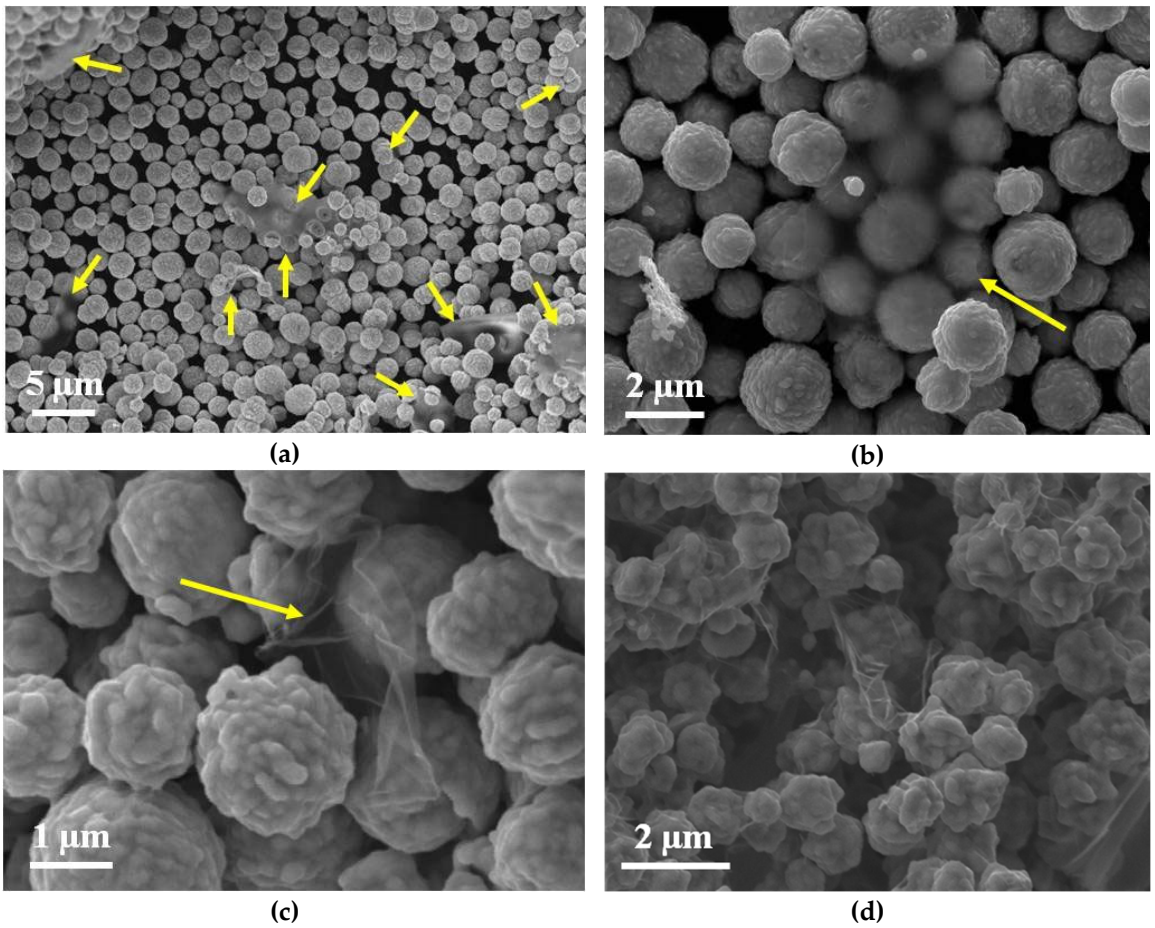

Figure 1. SEM micrographs (SE, E = 5 KV) of the Ag/rGO nano-composite powder at different rGO concentration: **(a)** 0.5 vol.%; **(b)** and **(c)** 1 vol.%; and **(d)** 5 vol.%. Yellow arrows show rGO nano-reinforcements.

For higher concentration (i.e., 5 vol.%), the Ag particle size decreases down to 1 μm and presents a less spherical shape (Figure 1 (d)) in comparison with Ag particles fabricated with smaller rGO concentration (1 vol.% in Figure 1 (b)). One explanation of this evolution is linked to the nucleation rate of Ag at high GO concentration. When the GO concentration becomes important, heterogeneous nucleation of Ag on GO becomes predominant over homogenous nucleation. Also, the Ag reduction by AA is an auto-catalytic reaction, which means that a higher amount of Ag nucleus increases the

reaction rate. Both effects can explain the morphology change of the Ag particles with rGO concentration. Once, the Ag particles precipitated, the aqueous suspension was heated to 90 ºC for 1 h to induce the GO reduction. As can be seen in Figure 1 (a) to (c) a concentration comprises between 0.5 to 1 %.vol allows a homogenous dispersion of the nano-reinforcements in the Ag matrix (yellow arrows). However, above 1 vol.% of rGO, a network of interconnected rGO sheets surround the Ag particles Figure 1 (d).

The effect of GO reduction using hydrazine or ascorbic acid has been studied by Raman spectroscopy Figure 2 (a) displays the Raman spectrum of the as-received GO and rGO reduced by AA or hydrazine, respectively.

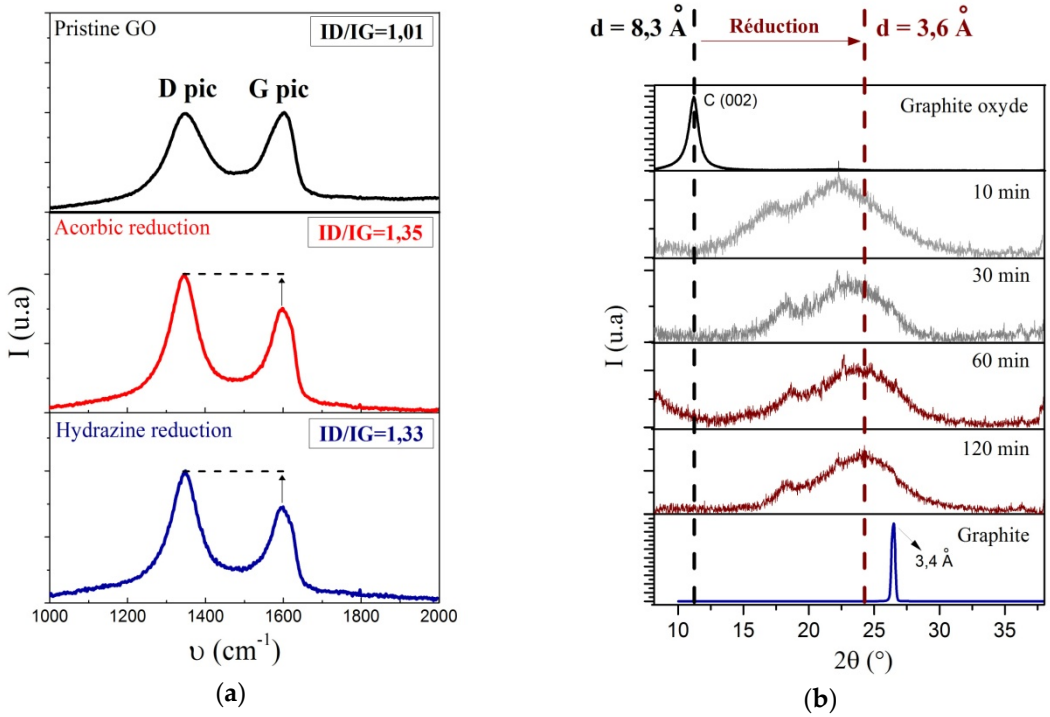

Figure 2. (a) Raman spectrum of pristine GO provided by KNANO® (black curve), rGO reduced by ascorbic acid at 90 °C for 1 h (red curve) and rGO reduced by hydrazine (blue curve) and **(b)** diffractograms of pristine GO (black curve), GO reduced by ascorbic acid at 90 °C for 10, 30, 60 and 120 min (grey and red curves) and graphite (blue curve).

On each spectrum, a D-band is observed at a wavenumber of 1350 cm^{-1}, which is related to defect or disorder in the carbon structure (sp3 carbon) and a G-band at 1580 cm^{-1} which results from order graphite (sp2 carbon) [35]. Due to the fact that the intensity of the I_D peak in related to "number" of defect (sp3 carbon) and the I_G peak to the number of order carbon (sp2 carbon) the I_D/I_G ratio is commonly used to evaluate the quality of the reduction of GO (the higher the ratio the higher the quality of the graphite). It can be observed that the I_D/I_G ratio is 1.01 for GO and increase after GO reduction to 1.34.

The same increase was reported in previous work on the chemical reduction of GO [30, 31, 36, 37]. The I_D/I_G increases resulted from a decrease in the average size of Csp^2 domains [38, 39] and to an

increase in the distance between the Csp^3 defect domains [39]. Moreover, the I_D/I_G ratio of the rGO reduced by either ascorbic acid or hydrazine are equivalent implying similar reduction level, as reported in other studies [30, 31, 36, 37]. Furthermore, the GO reduction rate by AA was monitored by measuring the inter-layer distance via XRD at different times. Figure 2 (b) presents the diffractograms of the GO, the rGO from 10 to 120 min at 90 ºC and the graphite. The diffractogram of the as-received GO shows a peak at $2\theta = 11^\circ$ and has an interlayer distance of 8.3 Å. The rGO has a diffraction peak around $2\theta = 22.5$ to 24° depending on the reduction time, which corresponds to the (002) plane of the hexagonal carbon structure. Note that the low signal-to-noise ratio observed on the rGO is due to the presence of only a few G layers after the exfoliation steps. The interlayer distance measured on the GO rapidly decrease from 8.3 Å down to 4.2 Å after only 10 min of reduction (i.e., 2θ shift toward high angles), then slowly decreases to 3.6 Å after 60 min. No change was observed after 120 min of reduction which implies that 60 min is the optimal reduction time. The diffractogram of pure graphite shows a diffraction peak at $2\theta = 26^\circ$, which corresponds to an interlayer distance of 3.4 Å. The disparity between the graphite and rGO interlayer distance can be explained by the fact that the reduction of GO is never completed, and some residual oxygen will remain on it, thus inducing a variation on the interlayer distance. These results are comparable with the one obtained for a conventional MLM using hydrazine as reported by others [44]–[46], [50]–[52], and demonstrate that AA is a suitable reducing agent to form rGO by a green MLM process.

Fabrication of Ag/rGO nanocomposites

After the green MLM process, the Ag/rGO composites powders were consolidated by hot pressing at 625 ºC for 25 min and with a pressure of 60 MPa. No evolution of the composite material density is observed for a rGO concentration between 0 to 5 vol.% with a density of about 98.5%.

The nanocomposites were cut and polished for SEM analysis, as present in Figure 3(a) to (d). The microstructure analysis reveals that the concentration of agglomerate increases in respect to the concentration of rGO in the materials. Besides, composites synthesis by hot pressing often results in a preferential orientation of the reinforcement perpendicular to the compression axis [40–42]. The same tendency is observed here, as shown in Figure 3 (e). The SEM micrographs after deep etching demonstrate a preferred orientation of the rGO agglomerates perpendicular to the compression axis. Nonetheless, as shown in Figure 3 (f), individual rGO sheets are located at the Ag grain boundary and therefore have the same orientation as the boundaries.

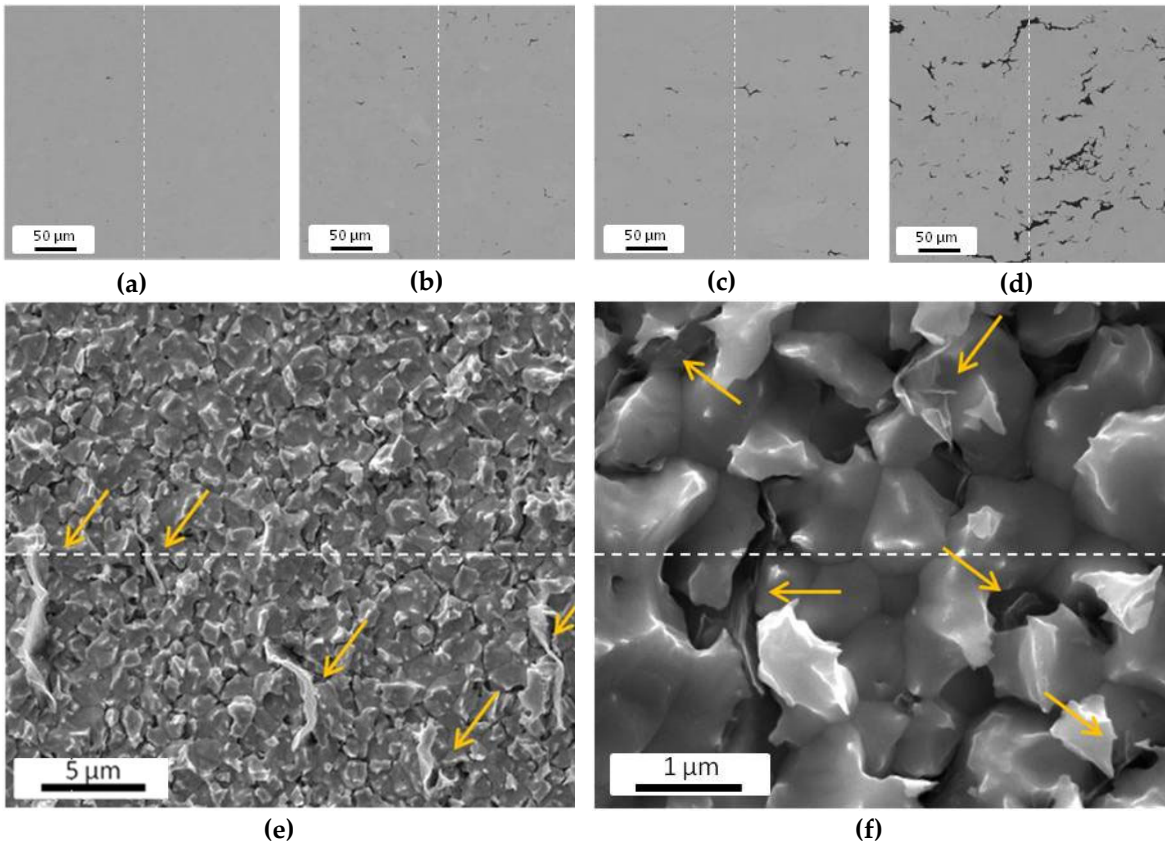

Figure 3. SEM micrographs (SE, E = 10 kV) of the cross-section of Ag/rGO composite material loaded to **(a)** 0.25 vol.%, **(b)** 0.5 vol.%, **(c)** 2 vol.%, **(d)** 5 vol.% in rGO and **(e)**-**(f)** SEM micrograph (SE, E = 5 KV) of the cross-section of an Ag/rGO composite material with 2.5 vol.% rGO concentration. The white axis corresponds to the compression axis of material, the yellow arrows correspond to **(e)** rGO micro agglomerates and **(f)** individualized rGO sheets.

The presence of nano reinforcements in the matrix may influence the Ag grain growth and their orientations, which could affect the thermal and especially the mechanical properties. The influence of rGO sheets on the microstructure of Ag was investigated by EBSD on pure Ag and Ag containing 0.5 and 2.5 vol.% of rGO. Figure 4 (a) displays the EBSD image of the pure Ag sample.

It can be seen that the Ag grains have an ellipsoidal shape and are randomly oriented with an average size of about 1.2 µm. Also, the size disparity is comprised of 0.1 to 2 µm. The addition of 0.5 vol.% of rGO does not influence the average size (1.18 µm), but a more significant size disparity is observed and comprise between 0.1 to 5 µm. An rGO concentration greater than 1% conducts to a decrease of the average grains size of 0.5 µm with a homogenous grains size disparity (Figure 4 (c)). The evolution of the Ag microstructure at a low rGO concentration (i.e., 0.25 and 0.5 vol.%) can be explained by two phenomena. First, due to a preferential recrystallization of Ag grains around the rGO, known as the particles simulated nucleation effect (PSN) [43–45]. Then, during the cooling stage the Ag matrix undergoes deformations which are induced by a coefficient of thermal expansion mismatch between Ag and rGO. Both effects individually or combined, could explain the grains size evolution at low rGO concentration. At higher rGO concentrations, above 1 vol.%, the refinement of the Ag

microstructure can be induced by a recrystallization delay due to a small distance between rGO agglomerates and defined at the Zener effect [43]. Besides, the large amount of rGO, located at the grain boundary between Ag grains, will limit the growth of the Ag grains by surface diffusion, and a finer microstructure is observed.

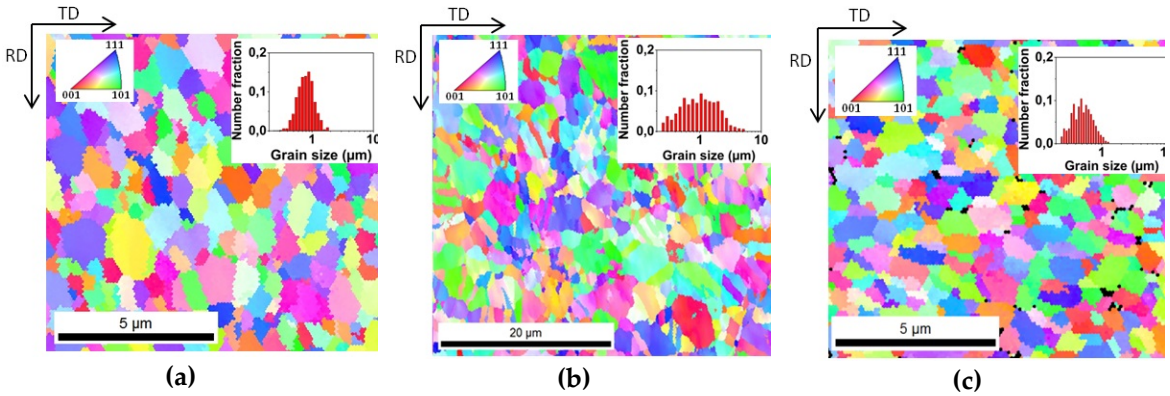

Figure 4. Inverse pole figure mapping and associated grain size of **(a)** pure Ag produced by MLM and composite material Ag/rGO concentrated at **(b)** 0.5 vol.% and **(c)** 2.5 vol.%.

Mechanical and thermal properties of Ag/rGO nanocomposites

To go further, the mechanical properties of the Ag/rGO nanocomposites were investigated at different rGO concentrations. First, the fracture behaviors of nanocomposites were studied for an rGO composition comprise between 0.5 to 5 vol.%. The SEM micrographs of the fractured composite containing 0.5 vol.% of rGO show a typical transgranular fracture, which is related to ductile behavior (Figure 5 (a) and (b)). The Ag/rGO composite having 1 vol.% of rGO shows a mixture of trans and intergranular fracture, which is assimilated to an intermediate state between ductile and brittle behavior (Figure 5 (c) and (d)). At higher rGO concentration (2.5 vol.%), an intergranular fracture is observed, as shown in Figure 5 (e) and (f), which is characteristic of a brittle behavior. Additionally, rGO sheets can be observed for an rGO concentration of 1 and 2.5 vol.% and result from the intergranular fracture of the Ag.

Hence, the introduction of rGO in the Ag matrix affect the grains sizes and morphology of Ag and thus change the Ag fracture behavior from ductile to brittle with an intermediate state for an rGO concentration of 1 vol.%.

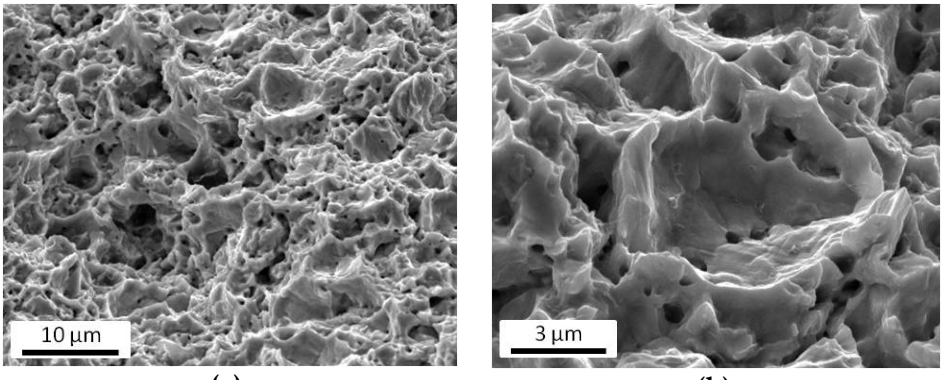

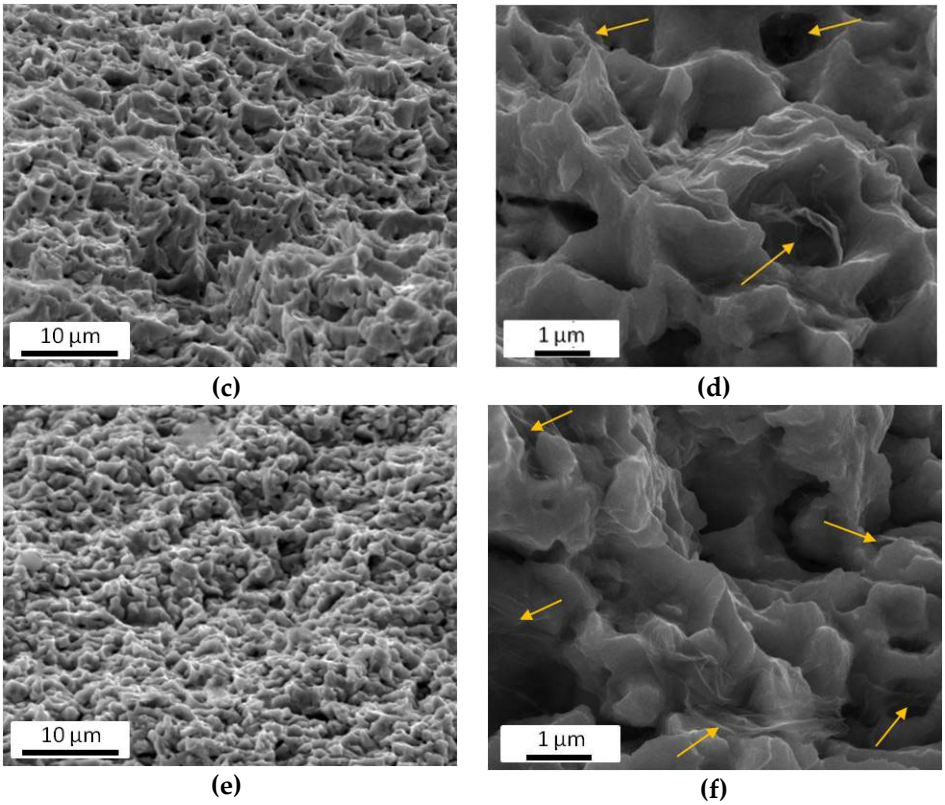

Figure 5. SEM micrographs (SE, E = 5 KV) of fracture surfaces of Ag/rGO composite materials with different rGO concentrations **(a)**-**(b)** 0.5 vol.%, **(c)**-**(d)** 1 vol.%, and **(e)**-**(f)** 2.5 vol.%. Yellow arrows show rGO nano-reinforcements.

Then, the apparent elastic modulus (E) and Vickers hardness (HV) were measured on pure Ag and on composite materials with an rGO concentration between 0.25 to 5 vol.% (see Figure 6). The evolution of the E shows that, for a low rGO concentration (0.25 to 0.5 vol.%), a decrease of the modulus down to 65 GPa is observed. At higher rGO concentration, the elastic modulus increases and reaches a maximum of 93 GPa and then decreases to 85 GPa for rGO concentration of 1 vol.% and 5 vol.%, respectively.

Moreover, the hardness of the nanocomposite follows similar trend for low concentrations comprises between 0.25 to 0.5 vol.% (decreased of HV) but differs for higher concentration. A maximum of 93 HV is reached at 2.5 vol.% of rGO, and then, the HV decreases as saw for the elastic modulus.

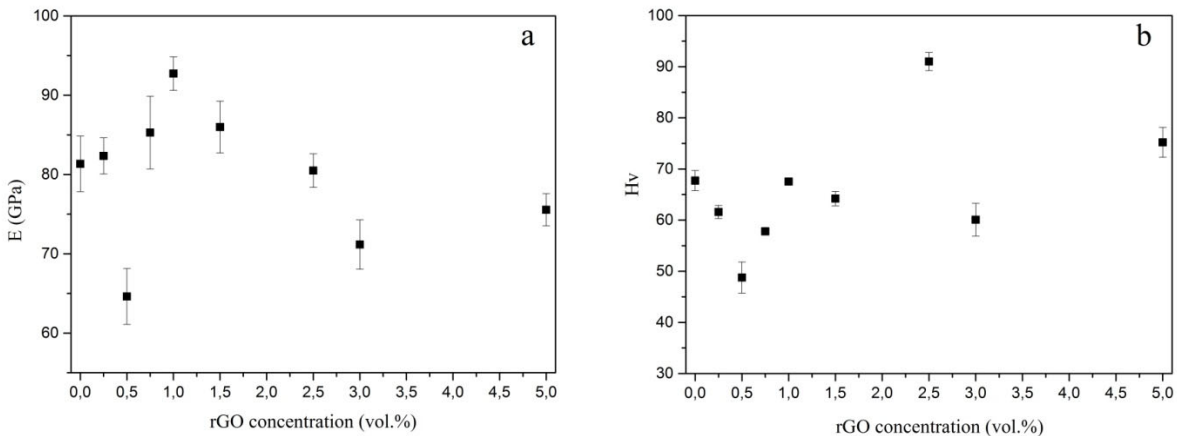

Fig. 6: Mechanical properties of Ag/rGO composite materials as a function of rGO concentration **(a)** elastic modulus and **(b)** Vickers micro-hardness.

These results were expected based on the previous microstructural and fracture behaviors analysis. As seen in the previous section, a low rGO concentration (0.1% to 0.5 vol.%) induced preferential recrystallization of the Ag grains around the rGO, which led to a broad distribution of Ag grains and a softening of the matrix. At higher concentration (0.75 to 1 vol.%), a homogenous and fine Ag microstructure was observed with the presence of rGO sheets in Ag grains and grain boundaries. The rGO sheets, located at the Ag grain boundaries, inhibit the boundary diffusion phenomena necessary for the recrystallization of the Ag matrix and harder the materials. On the other hand, the rGO located inside the grains promotes the elastic modulus by inducing a load transfer from the matrix to the rGO. However, when the reinforcement concentration becomes too important (> 2.5 vol.%), a large number of rGO agglomerates formed in the matrix and degrade the mechanical properties.[9, 13, 17, 21].

It must be mentioned that the elastic modulus reaches its maximum value for an rGO concentration of 1 vol.% (93 GPa) while the hardness is maximum for a concentration of 2.5 vol.% (91 Hv). These values have to be correlated with the morphology of the fracture surfaces. Indeed, for an rGO volume fraction of 2.5%, the rupture behavior, linked with granular debonding and the absence of a cup, have to be associated with the decrease of the ductility and the increase of the hardness of the Ag/rGO composite material, compared to pure Ag. For an rGO volume fraction of 1%, a ductile fracture surface is observed associated with a cup like structure. Besides, the cup size is smaller than those observed in materials with a lower concentration of rGO.

In addition, the presence of rGO sheets at the bottom of the cups (yellow arrows in Figure 5 (d)) may explain the increase in the elastic modulus of the materials associated with a load transfer between the matrix and the reinforcements. Thus, granular refinement of the matrix would be the main cause of the increase in hardness of Ag/rGO materials, while load transfer between the matrix and the rGO would be the cause of the increase in their elastic modulus. This would explain why the maximum of these two parameters is not reached for the same rGO concentration. It should also be noted that the maximum hardness of 91 HV is obtained for a concentration of 2.5 vol.% of rGO, which is close to the optimal rGO volume fraction reported *Hao and al.* [9] with a hardness of 76 Hv at 2.3 vol.% rGO.

Additionally to the mechanical measurements, the thermal properties of Ag/rGO nanocomposite were studied in the longitudinal and transverse directions. It can be observed that for a low rGO concentration (0.1 to 1 vol.%) the longitudinal TC is close to pure Ag with a value of 395 W/m.K but the transversal TC decreases down to 375 W/m.K. The decrease of the transverse TC is may be

associated with the alignment, during the HP process, of the rGO perpendicular to the compassion axis, leading to the fabrication of an anisotropic composite. At higher rGO concentration (> 1 vol.%), the TC decreases linearly with respect to the amount of rGO and the TC anisotropy increases. As seen before, the number of agglomerates increases when the rGO concentration increases and these agglomerates are oriented perpendicularly to the compression axis of the materials. In this case, the heat transfer in the composite is governed between the Ag matrix and the rGO agglomerates resulting from degradation of the thermal properties.

Conclusions

In this paper, a green MLM process is developed to synthesize Ag/rGO nanocomposites. It has been demonstrated that the substitution of hydrazine by AA allows obtaining the same experimental results in terms of reduction rate and mixture homogeneity. Also, the used of AA enables us to separate the Ag and rGO reduction/precipitation by merely varying the solution temperature (i.e., ambient to 90 ºC). The synthesized Ag powders by green MLM appeared to be spherical and monodispersed for a GO concentration below 3 vol.%.

The fabrication of Ag/rGO composite by hot pressing led to dense composite materials with homogenous dispersion of the nano-reinforcement for an rGO concentration lower than 1 vol.%. The fracture behavior of Ag can be tailored from a ductile to brittle fracture depending on the amount of rGO in the matrix. Besides, the preferential orientation of the nano-reinforcement conducts to an improvement of the elastic modulus up to 16% while being as hard as pure Ag. Also, it was shown that the TC of the Ag/rGO containing 1 vol.% of rGO is almost not affected in the longitudinal direction compare to pure Ag with a value of 395 W/m.K.

The process developed in this work has the potential to be used on a large scale and reduced the environmental impact of toxic chemical components. The fabrication of nanocomposites by green MLM followed by hot pressing enables to tailor the mechanical properties and fracture behavior of Ag/rGO composite materials without degrading the high TC of Ag.

Data available statement: The datasets generated during and/or analyzed during the current study are available from the corresponding author on reasonable request.

Conflicts of Interest: The authors declare no conflict of interest. The funders had no role in the design of the study; in the collection, analyses, or interpretation of data; in the writing of the manuscript, or in the decision to publish the results.

317

References

1. Joshi PB, Ramakrishnan P (2004) Materials for electrical and electronic contacts : processing, properties, and applications. Science Publishers

2. Lin Z, Liu S, Sun X, et al (2014) The effects of citric acid on the synthesis and performance of silver-tin oxide electrical contact materials. J Alloys Compd 588:30–35. https://doi.org/10.1016/j.jallcom.2013.10.222

3. Jiang Y, Liu SH, Chen JL, et al (2015) Preparation of rod-like SnO2 powder and its application in Ag-SnO2 electrical contact materials. Mater Res Innov 19:S152–S156. https://doi.org/10.1179/1432891715Z.0000000001535

4. Ćosović V, Ćosović A, Talijan N, et al (2013) Improving dispersion of SnO2 nanoparticles in Ag-SnO2 electrical contact materials using template method. J Alloys Compd 567:33–39. https://doi.org/10.1016/j.jallcom.2013.03.094

5. Guzmán D, Muñoz P, Aguilar C, et al (2014) Synthesis of Ag–ZnO powders by means of a mechanochemical process. Appl Phys A Mater Sci Process 117:871–875. https://doi.org/10.1007/s00339-014-8447-7

6. Rehani BR, Joshi PB, Kaushik VK (2009) Nanostructured silver-graphite electrical contact materials processed by mechanical milling. Indian J Eng Mater Sci 16:281–287

7. Pietrzak K, Gładki A, Frydman K, Wójcik-grzybek D (2016) Electrical properties of Ag-C and Cu-C contact materials. Electron Mater T.44:4–10

8. Borkowski P, Walczuk E (2010) Electrical properties of Ag-C contact materials containing different allotropes of carbon. In: Electrical Contacts, Proceedings of the Annual Holm Conference on Electrical Contacts

9. Hao X, Wang X, Zhou S, et al (2018) Microstructure and properties of silver matrix composites reinforced with Ag-doped graphene. Mater Chem Phys 215:327–331. https://doi.org/10.1016/j.matchemphys.2018.05.036

10. Hsieh C-C, Liu W-R (2017) Synthesis and characterization of nitrogen-doped graphene nanosheets/copper composite film for thermal dissipation. Carbon N Y 118:1–7. https://doi.org/10.1016/J.CARBON.2017.03.025

11. Chu K, Wang X, Wang F, et al (2018) Largely enhanced thermal conductivity of graphene/copper composites with highly aligned graphene network. Carbon N Y 127:102–112. https://doi.org/10.1016/j.carbon.2017.10.099

12. Hu Z, Tong G, Lin D, et al (2016) Graphene-reinforced metal matrix nanocomposites - A review. Mater Sci Technol (United Kingdom) 32:930–953. https://doi.org/10.1080/02670836.2015.1104018

13. Nieto A, Bisht A, Lahiri D, et al (2017) Graphene reinforced metal and ceramic matrix composites: a review. Int Mater Rev 62:241–302. https://doi.org/10.1080/09506608.2016.1219481

14. Che H, Xie H, Liang S, et al (2014) Highly enhanced mechanical properties in Cu matrix composites reinforced with graphene decorated metallic nanoparticles. J Mater Sci 49:3725–3731. https://doi.org/10.1007/s10853-014-8082-x

15. Tang Y, Yang X, Wang R, Li M (2014) Enhancement of the mechanical properties of graphene-copper composites with graphene-nickel hybrids. Mater Sci Eng A 599:247–254. https://doi.org/10.1016/j.msea.2014.01.061

16. Shao Z, Jiang Y, Jiang X, et al (2018) Recent Developments Concerning the Dispersion Methods and Mechanisms of Graphene. Coatings 8:33. https://doi.org/10.3390/coatings8010033

17. Gao X, Yue H, Guo E, et al (2016) Mechanical properties and thermal conductivity of graphene reinforced copper matrix composites. Powder Technol 301:601–607. https://doi.org/10.1016/j.powtec.2016.06.045

18. Rashad M, Pan FS, Asif M, Ullah A (2014) Improved mechanical properties of magnesium–graphene composites with copper–graphene hybrids. Mater Sci Technol 31:1452–1461. https://doi.org/10.1179/1743284714y.0000000726

19. Yue H, Yao L, Gao X, et al (2017) Effect of ball-milling and graphene contents on the mechanical properties and fracture mechanisms of graphene nanosheets reinforced copper matrix composites. J Alloys Compd 691:755–762. https://doi.org/10.1016/j.jallcom.2016.08.303

20. Pérez-Bustamante R, Bolaños-Morales D, Bonilla-Martínez J, et al (2015) Microstructural and hardness behavior of graphene-nanoplatelets/aluminum composites synthesized by mechanical alloying. J Alloys Compd 615:S578–S582. https://doi.org/10.1016/j.jallcom.2014.01.225

21. Saboori A, Pavese M, Badini C, Fino P (2018) A novel Cu-GNPs nanocomposite with improved thermal and mechanical properties. Acta Metall Sin (English Lett 31:148–152. https://doi.org/10.1007/s40195-017-0643-y

22. Bastwros M, Zhu C, Kim G-Y, et al (2014) Effect of ball milling on graphene reinforced Al6061 composite fabricated by semi-solid sintering. Compos Part B Eng 60:111–118. https://doi.org/10.1016/j.compositesb.2013.12.043

23. Ghosh G, Olson GB (2002) The isotropic shear modulus of multicomponent Fe-base solid solutions. Acta Mater 50:2655–2675. https://doi.org/10.1016/S1359-6454(02)00096-4

24. Huang YY, Terentjev EM (2012) Dispersion of carbon nanotubes: Mixing, sonication, stabilization, and composite properties. Polymers (Basel) 4:275–295. https://doi.org/10.3390/polym4010275

25. Kumar HGP, Xavior MA (2014) Graphene Reinforced Metal Matrix Composite (GRMMC): A Review. Procedia Eng 97:1033–1040. https://doi.org/10.1016/j.proeng.2014.12.381

26. Hwang J, Jeon S, Kim T-S, et al (2013) Enhanced Mechanical Properties of Graphene/Copper Nanocomposites Using a Molecular-Level Mixing Process. Adv Mater 25:6724–6729. https://doi.org/10.1002/adma.201302495

27. Pengpeng Wang, Zhijun Wei, Minhua Shen, Hui Pan, Jun Fu LC (2017) In-situ Synthesized Silver-graphene Nanocomposite with Enhanced Electrical and Mechanical Properties. IEEE Holm Conf Electr Contacts. https://doi.org/10.1088/1742-6596/240/1/012128

28. Lee B, Koo MY, Jin SH, et al (2014) Simultaneous strengthening and toughening of reduced graphene oxide/alumina composites fabricated by molecular-level mixing process. Carbon N Y 78:212–219. https://doi.org/10.1016/j.carbon.2014.06.074

29. Ickecan D, Zan R, Nezir S (2017) Eco-Friendly Synthesis and Characterization of Reduced Graphene Oxide. J Phys Conf Ser 902:6426–6432. https://doi.org/10.1088/1742-6596/902/1/012027

30. Zhang J, Yang H, Shen G, et al (2010) Reduction of graphene oxide via l -ascorbic acid. Chem Commun 46:1112–1114. https://doi.org/10.1039/B917705A

31. Fernández-Merino MJ, Guardia L, Paredes JI, et al (2010) Vitamin C Is an Ideal Substitute for Hydrazine in the Reduction of Graphene Oxide Suspensions. J Phys Chem C 114:6426–6432. https://doi.org/10.1021/jp100603h

32. Lightfoot EN, Bird RB, E. Stewart WE (1960) Transport Phenomena. John Wiley & Sons, Ltd

33. Oliver WC, Pharr GM (1992) An improved technique for determining hardness and elastic modulus using load and displacement sensing indentation experiments. J Mater Res 7:

34. Oliver WC (2004) Measurement of hardness and elastic modulus by instrumented indentation : Advances in understanding and refinements to methodology

35. Johra FT, Lee JW, Jung WG (2014) Facile and safe graphene preparation on solution based platform. J Ind Eng Chem 20:2883–2887. https://doi.org/10.1016/j.jiec.2013.11.022

36. De Silva KKH, Huang H-H, Yoshimura M (2018) Progress of reduction of graphene oxide by ascorbic acid. Appl Surf Sci 447:338–346. https://doi.org/10.1016/J.APSUSC.2018.03.243

37. Zainuddin MF, Him NRN, Othman NH, et al (2017) Review on effects of hydrazine hydrate and L-ascorbic acid on electrical conductivity of graphene. p 090004

38. Pei S, Cheng HM (2012) The reduction of graphene oxide. Carbon N Y 50:3210–3228. https://doi.org/10.1016/j.carbon.2011.11.010

39. Lucchese MM, Stavale F, Ferreira EHM, et al (2010) Quantifying ion-induced defects and

Raman relaxation length in graphene. Carbon N Y 48:1592–1597. https://doi.org/10.1016/j.carbon.2009.12.057

40. Chamroune N, Mereib D, Delange F, et al (2018) Effect of flake powder metallurgy on thermal conductivity of graphite flakes reinforced aluminum matrix composites. J Mater Sci 53:8180–8192. https://doi.org/10.1007/s10853-018-2139-1

41. Oddone V, Boerner B, Reich S (2017) Composites of aluminum alloy and magnesium alloy with graphite showing low thermal expansion and high specific thermal conductivity. Sci Technol Adv Mater 18:180–186. https://doi.org/10.1080/14686996.2017.1286222

42. Firkowska I, Boden A, Boerner B, Reich S (2015) The Origin of High Thermal Conductivity and Ultralow Thermal Expansion in Copper–Graphite Composites. Nano Lett 15:4745–4751. https://doi.org/10.1021/acs.nanolett.5b01664

43. Humphreys FJ, Hatherly M (2004) Recrystallization and related annealing phenomena. Elsevier

44. Humphreys FJ (1977) The nucleation of recrystallization at second phase particles in deformed aluminium. Acta Metall 25:1323–1344. https://doi.org/10.1016/0001-6160(77)90109-2

45. Porter JR, Humphreys FJ (1979) Nucleation of recrystallization at second-phase particles in deformed copper alloys. Met Sci 13:83–88. https://doi.org/10.1179/msc.1979.13.2.83